OPTICALLY INTERCONNECTED INTELLIGENT RAM MULTIPROCESSORS (OPTO-IRAM)

Georgia Institute of Technology

APPROVED FOR PUBLIC RELEASE; DISTRIBUTION UNLIMITED.

AIR FORCE RESEARCH LABORATORY
SENSORS DIRECTORATE
ROME RESEARCH SITE
ROME, NEW YORK

STINFO FINAL REPORT

This report has been reviewed by the Air Force Research Laboratory, Information Directorate, Public Affairs Office (IFOIPA) and is releasable to the National Technical Information Service (NTIS). At NTIS it will be releasable to the general public, including foreign nations.

AFRL-SN-RS-TR-2004-XX has been reviewed and is approved for publication

APPROVED: /s/

        JAMES R. HUNTER
        Project Engineer

FOR THE DIRECTOR: /s/

        GERARD J. GENELLO, Acting Chief
        Rome Operations Office
        Sensors Directorate

REPORT DOCUMENTATION PAGE

Public reporting burden for this collection of information is estimated to average 1 hour per response, including the time for reviewing instructions, searching existing data sources, gathering and maintaining the data needed, and completing and reviewing this collection of information. Send comments regarding this burden estimate or any other aspect of this collection of information, including suggestions for reducing this burden to Washington Headquarters Services, Directorate for Information Operations and Reports, 1215 Jefferson Davis Highway, Suite 1204, Arlington, VA 22202-4302, and to the Office of Management and Budget, Paperwork Reduction Project (0704-0188), Washington, DC 20503

1. AGENCY USE ONLY (Leave blank)	2. REPORT DATE OCTOBER 2004	3. REPORT TYPE AND DATES COVERED Final Jun 98 – Mar 04

4. TITLE AND SUBTITLE
OPTICALLY INTERCONNECTED INTELLIGENT RAM
MULTIPROCESSORS (OPTO-IRAM)

6. AUTHOR(S)
Chung-Seok Seo and
Abhijit Chatterjee

5. FUNDING NUMBERS
C   - F30602-98-2-0248
PE - 62712E
PR - A287
TA - 00
WU - 01

7. PERFORMING ORGANIZATION NAME(S) AND ADDRESS(ES)
Georgia Institute of Technology
School of Electrical and Computer Engineering
777 Atlantic Drive, NW
Atlanta Georgia 30332-0250

8. PERFORMING ORGANIZATION REPORT NUMBER

N/A

9. SPONSORING / MONITORING AGENCY NAME(S) AND ADDRESS(ES)
Defense Advanced Research Projects Agency   AFRL/IFSNDP
3701 North Fairfax Drive   25 Electronic Parkway
Arlington Virginia 22203-1714   Rome New York 13441-4515

10. SPONSORING / MONITORING AGENCY REPORT NUMBER

AFRL-SN-RS-TR-2004-282

11. SUPPLEMENTARY NOTES

AFRL Project Engineer: James R. Hunter/SNDP/(315) 330-7045/ James.Hunter@rl.af.mil

12a. DISTRIBUTION / AVAILABILITY STATEMENT
APPROVED FOR PUBLIC RELEASE; DISTRIBUTION UNLIMITED.

12b. DISTRIBUTION CODE

13. ABSTRACT *(Maximum 200 Words)*
Current electrical systems are faced with the limitation in performance by the electrical interconnect technology determining overall processing speed. In addition, the electrical interconnects containing many long distance interconnects require high power to drive. One of the best methods to overcome these bottlenecks is through the use of optical interconnect to limit interconnect latency and power. This report describes development of Computer Aided Design (CAD) tools for optimizing a new approach to high performance System-on-Chip (SoC) utilizing free-space optical interconnects technology. Two approaches to design and optimization of the optoelectronic systems using optical interconnections are presented.

14. SUBJECT TERMS
Optical Interconnects, Free-Space Optics, Optical Modeling, Optical Architectures, On-Chip Interconnects

15. NUMBER OF PAGES
48

16. PRICE CODE

17. SECURITY CLASSIFICATION OF REPORT UNCLASSIFIED	18. SECURITY CLASSIFICATION OF THIS PAGE UNCLASSIFIED	19. SECURITY CLASSIFICATION OF ABSTRACT UNCLASSIFIED	20. LIMITATION OF ABSTRACT UL

Table of Contents

List of Figures

List of Tables

1. Introduction

Current electrical systems are faced with the limitation in performance by the electrical interconnect technology determining overall processing speed. In addition, the electrical interconnects containing many long distance interconnects require high power to drive. One of the best ways to overcome these bottlenecks is through the use of optical interconnect to limit interconnect latency and power.

The 2002 Semiconductor Industry Association (SIA) roadmap update shows the substantial problems associated with electrical interconnects on silicon chips. Off-chip long distance interconnections suffer in performance [1]. It is proposed to replace such interconnections with optical interconnect to mitigate specific interconnect performance issues.

In 2000, D. A. B. Miller codified the physical advantages of optical interconnect over electrical interconnect [2]. Some possible practical advantages of optical interconnects are described in below.

- Design simplification:
  - No electromagnetic wave phenomena.
  - No distance dependence.
  - No frequency dependence.
- Architecture:
  - Large numbers of long high-speed connections.
  - 2D interconnect architecture.
  - No requirement of interconnect hierarchy.
- Timing:
  - Predictable signal timing.
  - No timing skew.
- Other physical advantages:
  - Power savings.
  - High interconnect density.

Because of the above advantages, optical interconnects could increase overall performance of electrical packages, and reduce the crosstalk, power consumption and signal latency. Due to the lack of computer-aided design (CAD) tools in optics, it necessitates the development of new CAD tools for emerging technologies such as optical interconnect.

2. Overview of Existing Work

In this section, the existing works about optical interconnect are presented. For a special case, the brief history of optical clock distribution is also presented.

2.1. Optical Interconnection

During 1960s, the semiconductor diode laser had been developed. This was the starting point that tried to use optics in digital computation. As the conclusion of the first demonstration, optical devices could not substitute for transistors in general computing machines because they consumed too much power [3]. However, the ideas of optics for communication were conceived at that time. From the mid 1970s to the late 1980s, the optical switching was paid attention because optical switch could be much faster than any electrical transistor [4]. This is still valid because nonlinear optics can make logic devices much faster than any electrical devices. In the early 1980s, quantum well structures were enhanced and this led to further interest in semiconductor optical switching devices.

In 1984, J. W. Goodman proposed ideas of optical interconnection of very large scale integration (VLSI) electronics: intra-chip data communications and inter-chip data communications. They were the actual start of the field of optical interconnects [5]. The quantum-confined Stark effect was discovered in III-V semiconductor quantum wells in 1984 [6]. This effect was important for optical computing and optical interconnects because of the allowance of low energy devices, the possibility of 2D interconnected modulator or switch and the capability of large arrays of devices. The very important devices, vertical cavity surface-emitting lasers (VCSELs), were developed [7] and demonstrated [8] in the late 1980s. The first demonstration which VCSEL was electrically pumped was successfully made at room temperature. VCSELs became very interested practical devices, especially for low-cost optical fiber connections. Moreover, they are candidate devices for optical interconnects to silicon chips.

An optomechanical configuration has been conceived [9] that is far less complex than any current approach in 1994. Implementing a Fourier-plane-based interconnect with an arbitrary degree of space variance, it comprises only two component aggregates requiring mutual alignment in free space. Connections among such free-space interconnected modules (FSIMs) are effected over waveguide ribbons in a natural fashion obeying the principles of hierarchical interconnections: all signals leave chips on the same physical transport medium, in this case through the optical array input and output (I/O) apertures to free-space modes. Use of a mechanically compliant medium (ribbons) decouples system scaling from free-space alignment requirements.

A prototype 3D optoelectronic neural network was implemented in 1994 [10]. It was composed of a 16-node input, 4-neuron hidden, and a single-neuron output layer. The prototype used high-speed optical interconnects for fan-out and mixed-signal VLSI circuits for fan-in. In 1997, S. P. Levitan, *et al*, developed "Chatoyant", a mixed-signal CAD tool for performing end-to-end system simulations of free space interconnection systems [11]. Chatoyant was able to analyze optical, electrical, and mechanical trade-offs. The prototype system for intra multi-chip module (MCM) interconnects was built in 1999 [12]. This system supported 48 independent free-space optical interconnect (FSOI) channels using 8 lasers and detectors. All chips were integrated on a ceramic substrate with three silicon chips.

M. Forbes, *et al*, presented three different types of approaches for optoelectronic interconnects between VLSI chips [13]: fibre-ribbons, planar waveguides and free-space optics. This paper pointed out the limitations of electrical interconnect and the advantages of optical interconnect.

Optical connections between individual computer systems are now available. N. Savage anticipated that optical interconnection would be introduced in the computer to connect circuit boards within 2-5 years [14] and connect chips within 5-10 years. Optical interconnects will be feasible in 15 years for on-chip interconnects.

2.2. Optical Clock Distribution

Claude Chappe invented optical telegraph in 1790s and it is the starting point of optical communication systems. In 1870, John Tyndall demonstrated that light was guided in a water jet.

However, the idea of a communication system based on the propagation of light through circular dielectric waveguides was considered from the mid-1960s, albeit some theoretical studies were performed in the early years of the present century [15, 16].

In 1984, J. W. Goodman suggested three optical clock distribution approaches [5]: index-guided, unfocused free-space and focused free-space optical interconnect. In index-guided optical interconnect, two types of waveguides, optical fibers and optical waveguides integrated on a suitable substrate, can be used. The two optical interconnect technologies provide a compact and planar packaging of the global optical clock distribution without diffractive components. In unfocused free-space optical interconnect, the optical signals carrying the clock signals broadcast to the entire electronic chip. Because detectors are located in the same distance at the focal point of the lens, there is no clock skew. A focused free-space optical clock distribution uses a holographic optical element. The holographic optical element acts as a complex grating.

In 1988, B. D. Clymer and J. W. Goodman presented the skew properties of an array of optical transimpedence receivers associated with a hologram-based focused free-space optical clock distribution [17]. The test circuit used 3 μm Metal Oxide Semiconductor Implementation System (MOSIS) technology with 18 optical receivers.

P. J. Delfyett, *et al*, introduced the mode-locked operation of a semiconductor laser system as a jitterless timing source [18]. They demonstrated the optical clock distribution of 1024 separate ports utilizing optical fibers. The total accumulated timing jitter was less than 12ps.

A board-level free-space optical clock distribution system implemented with substrate mode hologram was presented by J. H. Yeh, *et al* in 1995 [19]. The system used an H-tree clock distribution to avoid clock skews. With 622MHz clock signal, 36ps of timing jitter and less than 10ps of clock skew were achieved.

In 1998, Y. Li, *et al*, reported board-level large bandwidth optical clock distributions with fanout of 128 on a printed circuit board using silica and polymer optical fibers [20]. The result showed the multi Gbps bandwidth capability.

A multi-GHz optical clock distribution on a Cray T-90 supercomputer multi-processor board is presented in 1999 [21]. The optical clock signal is distributed to 48 fanout points on

$14.5 \times 27 \text{cm}^2$ printed wiring board through a polyimide optical waveguide organized as an H-tree structure.

Optical clock distribution technology eliminates the disadvantages of electrical clock distribution such as clock skew, timing jitter, etc. Moreover, it allows no limitations on the maximum frequency of modulation of an optical signal.

3. The CAD Tools for Optoelectronic Systems

3.1. GOETHE (Generic Opto-Electronic system design THEurgist)

A CAD tool, GOETHE (Generic Opto-Electronic system design THEurgist), was developed for optimizing System-on-Chip (SoC) placement and routing of electrical and optical interconnects simultaneously utilizing free-space optical interconnect technology. GOETHE determines which of the interconnects are routed electrically and which are routed optically without exceeding the routing capacity of the optical interconnect while minimizing total electrical interconnect length. Free-space optical interconnect technology is suitable for routing on-chip interconnects using an optical interconnect layer [5]. Data throughput between modules could be enhanced through the use of free-space optical interconnect by a factor of a thousand [14].

This research discusses the design of the circuit on silicon substrate and its interaction with the optical substrate in Figure 1.
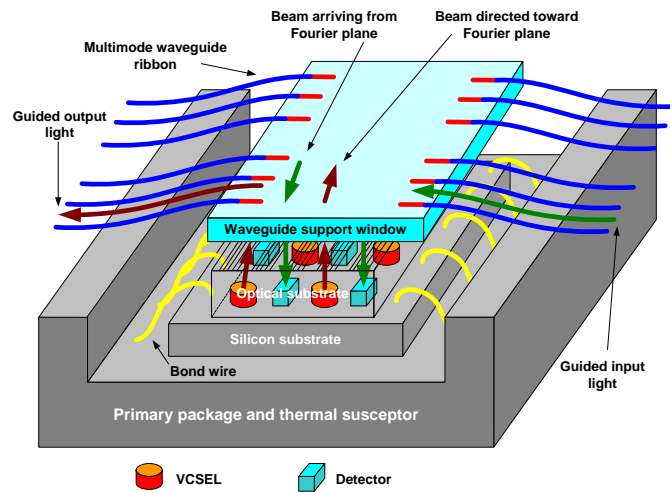
Figure 1. Optomechanical configuration in the neighborhood of the substrate

The integration configuration for optoelectronic substrate modules is shown in Figure 2. On the silicon substrate, VCSEL and photodetector array is bonded based upon flip-chip technology. On the optical substrate, there is a microoptical substrate which carries focal-plane diffractive elements.
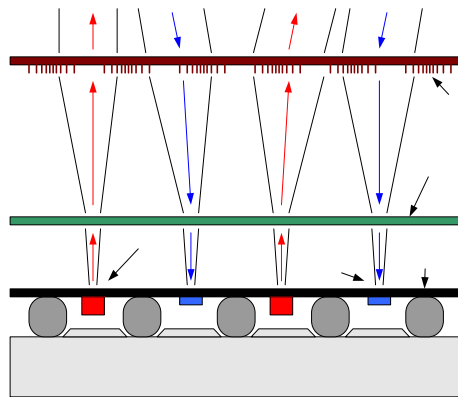
Figure 2. Integration configuration for optoelectronic substrate modules

3.1.1. Assumption

All module shapes are assumed to be rectangular-shaped. Pins are assigned into module periphery. A set of netlists are generated randomly for a specified number of modules. It is also assumed that the SoC operations are pipelined and that all module data transfers are buffered.

In this research, three arrangements of optical sensors are considered (see Figure 3). The gray circles represent emitters and the white circles represent detectors.

(a)　　　　　　　　　(b)　　　　　　　　　(c)

Figure 3. Three different sensor arrangements
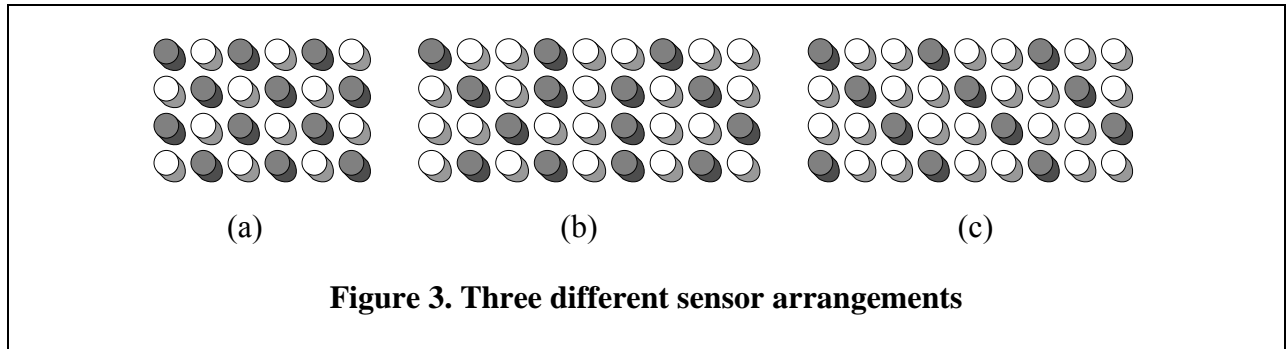
In the horizontal and vertical directions, the patterns of Figure 3 are repeated up to the size of a SoC. However, any regular sensor arrangements of emitter-detector configurations can be specified as an input to the CAD tool. Therefore, it is possible to experiment with different sensor arrangements of emitter-detector configurations so that determines which gives the best performance.

3.1.2. Optimization Algorithms

The optimization goals are as follows:

- *Given*: The preliminary locations of all modules and netlists and the arrangements of optical sensors in the VCSEL array.
- *Determine*: The optimal placement of all modules.
- *Such that (optimization criteria)*: (a) total electrical interconnect length is minimized and (b) the utilization of the optical routing capacity is maximized.

The optimization algorithm consists of a *placement and routing* and a *module compaction* step. These are described in Section 3.2.1 and 3.2.3.

3.1.2.1. Placement and Routing

Genetic Algorithm is employed in order to optimize placement of modules and routing of electrical and optical interconnects simultaneously. There are three steps to find the best placement of modules which gives minimum routing cost.

First of all, *population* is generated as a group of many random orders of modules. The number of populations is one of the inputs to the CAD tool. These orders are stored as a sequence of numbers. Second, two better groups which are called parents in the population and combine them to create two new solutions which are called children using *Crossover*. During crossover, a random point is picked in the parents' sequences and switched every number in the sequence after that point. When the placement of modules is changed, the sequence of the longest interconnects is also changed.

However, the crossover sometimes may not work because the population is represented by a sequence of numbers. An example is shown below [22].

Parent 1	1 2 3 4 5 **6 7 8 9**
Parent 2	8 7 6 3 2 **5 4 9 1**
Child 1	1 2 3 4 5 **5 4 9 1**
Child 2	8 7 6 3 2 **6 7 8 9**

Figure 4. An example that crossover operation does not work

To resolve this phenomenon, *partially matched crossover* is employed which is shown in Figure 5.

Parent 1	1 **2 3 4 5** 6 7 8 9
Parent 2	8 7 6 **3 2 5 4** 9 1
Child 1	1 **3 2 5 4** 6 9 8 7
Child 2	8 7 6 **2 3 4 5** 9 1

Figure 5. Partially matched crossover

Finally, modules are rotated to randomly chosen direction during *Mutation.*

The above operations may not reproduce good parents to better children. Therefore, if the children are not better than their parents, the children should be then discarded in the population. This decision is made by total routing cost (see Figure 9).

The algorithm attempts to replace long electrical interconnects with optical interconnects in the sequence of interconnect length. However, the breakpoint which electrical interconnect can be replaced with optical interconnect should be determined because electrical interconnects is still dominant over optical interconnects for very short distance interconnect. It is described in Section 3.1.2.5 and 3.1.2.6.

The following operations are the overall goals of the optimization.

- *Maximization of the utilization of the optical routing capacity.*
- *Minimization of the length of the critical (longest) electrical interconnects.*
- *Minimization of the total electrical interconnect length.*

If an input port of one module is to be routed to an output port of another module optically, then the input port and the output port must first be routed electrically to the nearest detector and emitter respectively. The cost of routings electrically from I/O ports to the sensors is included in the total cost of the electrical interconnect routing.

Figure 6 shows the CAD tool layout after the optimization with 16 modules.
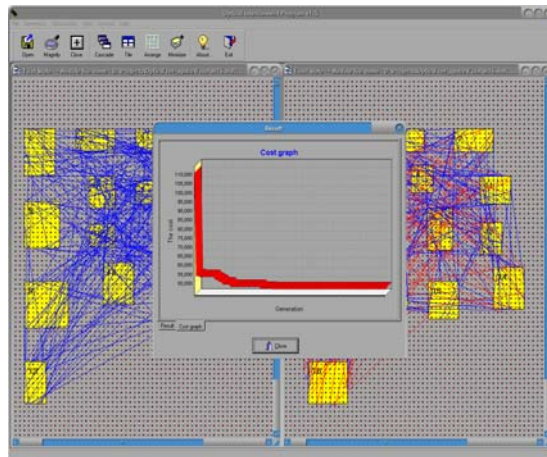
Figure 6. The CAD tool layout with optimization

3.1.2.2. Optical Routing Capacity

The physical length of optical interconnect does not matter. This is different from electrical interconnects. The optical routing capacity is determined by the number of optical directions in which signals have to be routed [9]. It turns out that due to the manner in which the diffraction grating of Figure 2 is fabricated, the optical routing capacity depends upon the number of optical directions rather than upon the number of physical routings of optical interconnects. Thereby, the number of optical directions that the optical substrate can support is one of the inputs to the optimization tool.

Figure 7(a) shows the physical routing of signals in the optical substrate. The gray circles represent emitters and the white circles represent detectors. Figure 7(b) shows optical vectors that the routing configuration of Figure 7(a) reduces to. All parallel optical directions in Figure 7(a) trim down to a single optical vector in Figure 7(b).

(a)   (b)

Figure 7. Optical vectors in Fourier plane
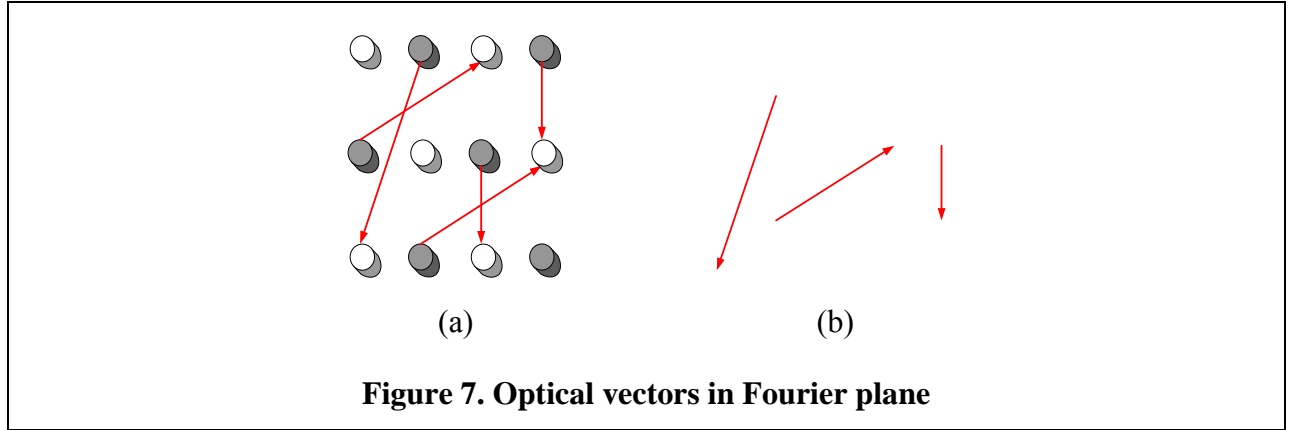
3.1.2.3. Module Compaction

The regions between modules are called *channels*. At the beginning of the optimization process, the CAD tool places modules with distance of wiring capacity. Then, virtual vertical direction lines are placed in the channels. The number of horizontal electrical interconnects crossing the vertical direction line for each channel is calculated. From this calculation, a difference between the wiring capacity and the wiring density, which we call *Ridge* is formed. The *Compression-Ridge method* is applied to delete the Ridge region [23]. This method is consecutively introduced in the horizontal direction.

Figure 8. Compression-Ridge Method
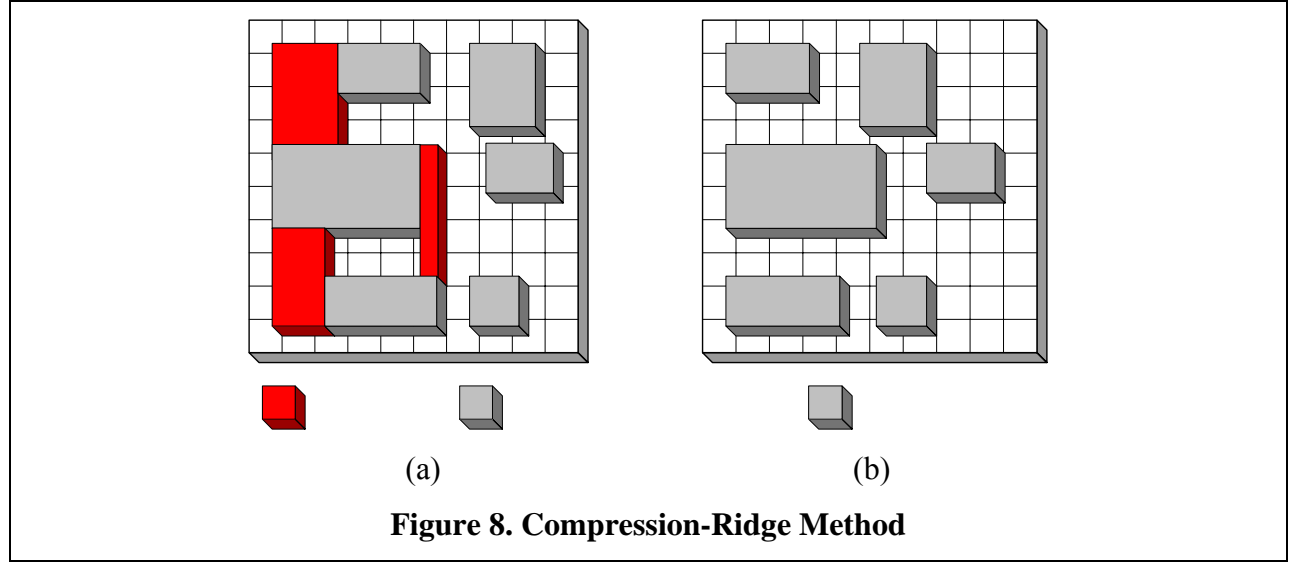
3.1.2.4. Cost Function

The cost function for the optimization is described in Figure 9. It is composed of the electrical interconnect cost and the optical interconnect cost. The first term includes the electrical interconnect length due to all the electrical interconnect plus the interconnect length contributions due to the electrical interconnects to all emitters and detectors which are occupied by optical interconnects. *Manhattan distance* is employed to calculate the electrical interconnect length.

$$Cost = \sum \left(Electrical\ interconnect\ length \right) + w\left(\frac{v}{D} \right)$$

$$where \begin{cases} w = \text{Weight factor for optical cost} \\ v = \text{The number of optical vectors in current layout} \\ D = \text{The maximum number of optical directions} \\ \quad \text{that the optical substrate can accommodate} \end{cases}$$

Figure 9. The cost function

The second term represents the optical interconnect cost. It attempts to maximize utilization of the optical routing capacity without exceeding it – note that at each step of the algorithm the longest interconnects are replaced with optical interconnect. *w* is the weight factor for the optical

11

cost and is set to be 100 in this research. It turns out that the optical cost is the percentage of the utilization of the optical routing capacity.

3.1.2.5. Speed Regression Model

In 1998, G. I. Yayla presented comparison of electrical interconnects and optical interconnects from the viewpoint of speed and energy consumption [24]. The results interested in this research is the comparison of off-chip electrical interconnect and free-space optical interconnect. The polynomial regressions are performed as functions of interconnect length on the extracted data from [24].

The speed regression models for the electrical interconnect and the optical interconnect are shown in Figure 10. The unit of interconnect length is cm and the unit of speed is MHz.
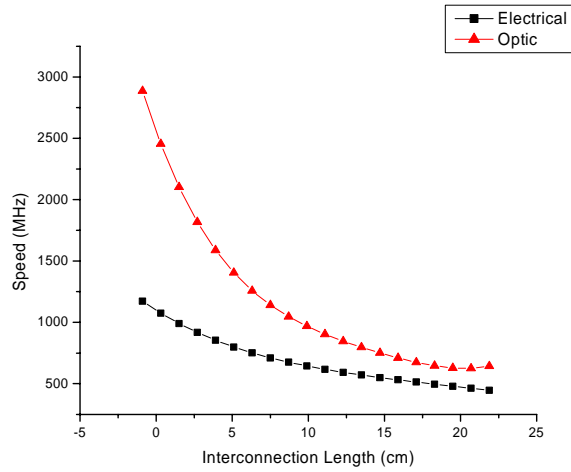
Figure 10. Speed regression models for the electrical interconnect and the optical interconnect

Equation (1) and (2) represent the speed of electrical interconnect and the speed of optical interconnect respectively, where x is interconnect length (cm).

$$Electrical = ax^4 - bx^3 + cx^2 - dx + e \qquad (1)$$

$$Optical = ax^4 - bx^3 + cx^2 - dx + e \qquad (2)$$

12

The coefficients of the speed regression models are shown in Table 1.

Table 1. Coefficients for speed regression models

Coefficient / Interconnect	a	b	c	d	e
Electrical	0.002	0.139	4.463	78.005	1098.28
Optical	0.022	1.255	28.649	341.929	2554.27

From the speed point of view, the optical interconnect is always dominant over the electrical interconnect.

3.1.2.6. Energy Consumption Regression Model

Figure 11 shows energy consumption regression models for the electrical interconnect and the optical interconnect. From the graph, the breakpoint which optical interconnect is dominant over electrical interconnect in terms of energy consumption is obtained. It is about 2.7cm. Therefore, the tool could replaces electrical interconnects with optical interconnects when the interconnect length exceeds 2.7cm without exceeding the optical routing capacity.
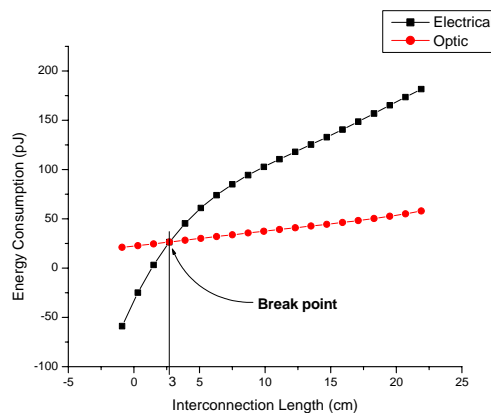
Figure 11. Energy consumption regression models for the electrical interconnect and the optical interconnect

The unit of interconnect length is cm and the unit of energy consumption is pJ. The polynomial regression models for the electrical interconnect and the optical interconnect are written by,

$$Electrical = -ax^4 + bx^3 - cx^2 + dx - e \qquad (3)$$

$$Optical = a \times (10^{-1}x)^4 - bx^3 + cx^2 + dx + e \qquad (4)$$

where x is interconnect length (cm).

Table 2 shows the coefficients of the regression models for energy consumption.

Table 2. Coefficients for energy consumption regression models

Coefficient Interconnect	a	b	c	d	e
Electrical	0.001	0.092	2.114	26.974	32.845
Optical	1.212	0.004	0.037	1.424	22.369

At the beginning and the end of optimization, the speed and the energy consumption are calculated with above analytical regression models to analyze the overall SoC performance.

3.1.2.7. Pseudo Code for Genetic Optimizer

The pseudo code for a genetic algorithm [25] with the objective of minimizing the total routing cost in a SoC is as follows:

```
Genetic_Algorithm_Objective( )
1.  Generate modules and netlists;
2.  Generate population; // Section 3.1.2.1
3.  Set the generation number;
4.  for (each  generation) {
5.      Partially matched crossover; // Section 3.1.2.1 – Swap modules
6.      Module compaction; // Section 3.1.2.3 - Find the optimal module placement
7.      Mutation; // Section 3.1.2.1 - Rotate modules
8.      Module compaction; // Section 3.1.2.3 - Find the optimal module placement
9.      Evolution; // Section 3.1.2.4 - Optimize the total routing cost
10. }
11. Calculate speed improvement; // Section 3.1.2.5
12. Calculate energy saving; // Section 3.1.2.6
13. Save result files;
```

Figure 12. Pseudo code for genetic optimizer

During *evolution*, the algorithm makes total cost minimal.

3.1.3. Results and Analysis

In this section, we present experimental results of the optimization achieved by using the CAD tool. All algorithms are implemented in C++.

3.1.3.1. Simulation Results

As mentioned in Section 3.1.1, a set of netlists was generated randomly for a specified number of modules. For comparison of overall SoC performance, cases with 9, 16, 25, 36 and 49 modules were simulated and a case of 36 modules is shown in this section. For the all simulations, the dimension of SoCs is set to be $10 \times 10 \text{cm}^2$.

Figure 13 shows the graph for the cost reduction versus the number of generations of the genetic optimizer with 36 modules and 1000 netlists. In this simulation, the optical routing capacity was 300.
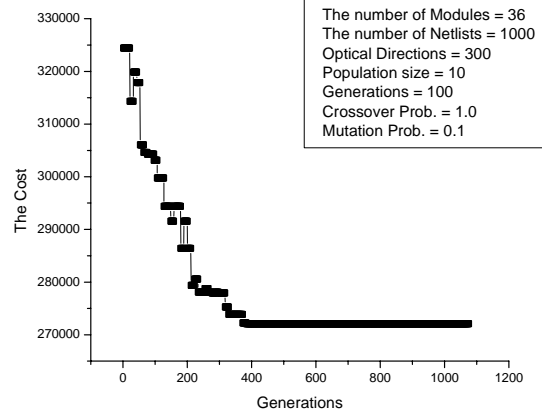
Figure 13. The cost graph

The result shows about 20% saving in the electrical cost which is given in Figure 9. About 99.7% of optical routing capacity is occupied.

Table 3 shows reductions in interconnect length for the different sensor distributions of Figure 3 with 36 modules and 1000 netlists. For the simulations, optical routing capacity was 500.

Table 3. Comparison with different sensor distributions

Arrangement	% of wires converted to optical links	% reduction in longest wire length	% reduction of total cost	No. of optical directions
(a)	50	60	69	495
(b)	48	52	65	475
(c)	43	47	62	428

Figure 14, Figure 15 and Figure 16 show an example of the optimization performed by the CAD tool. The blue lines represent electrical interconnects and the red lines represent optical interconnects. Figure 14 shows a layout and description of all the interconnects at the beginning of the optimization process.
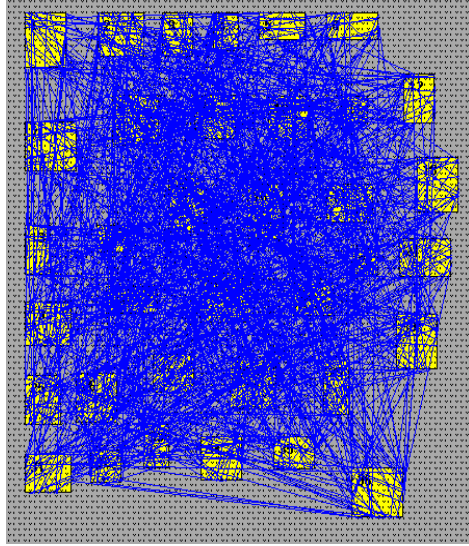
Figure 14. Routing without optimization

Figure 15 shows only the optical interconnects in the left side and only the electrical interconnects in the right side at the end of the optimization.
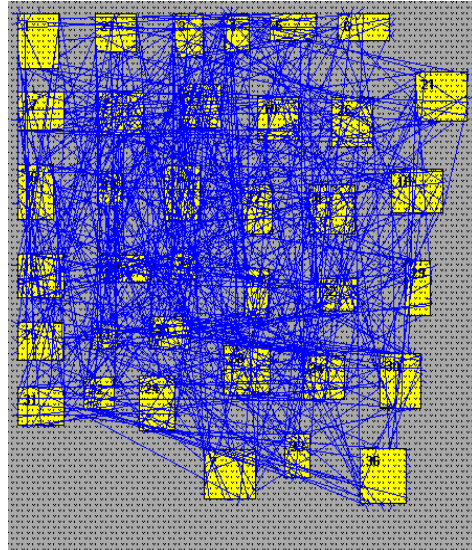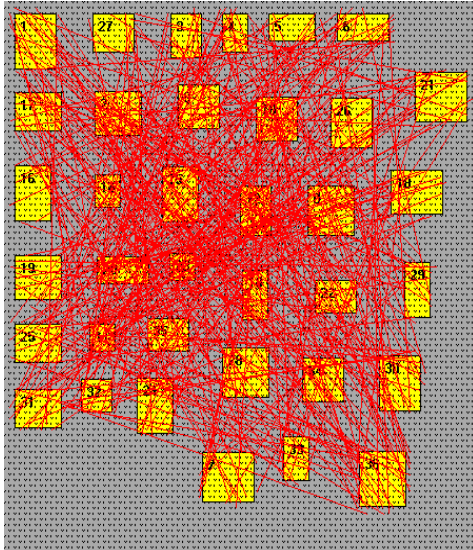
Figure 15. Optical routing and electrical routing with optimization

Another result for ARM core is shown in Figure 16. The first figure shows the routing result before optimization and the second figure shows only the optical interconnects and the third figure shoes only the electrical interconnects.
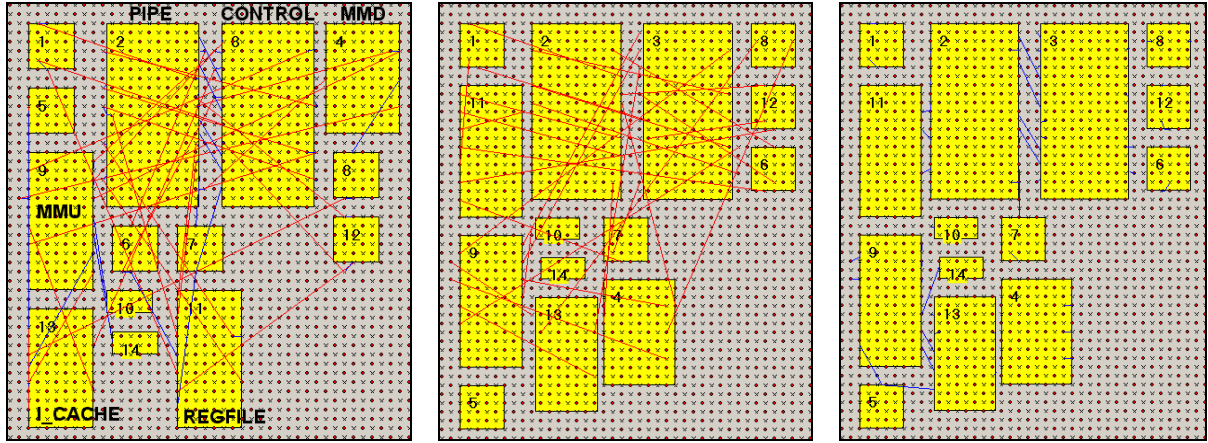
Figure 16. Routing result for ARM core

3.1.3.2. Speed and Energy Issues

In this section, we evaluate the SoC speed improvement and energy saving with 9, 16, 25, 36 and 49 modules. The graph for the percentage improvement of overall SoC speed versus the number of optical vectors with various numbers of modules is shown in Figure 17.
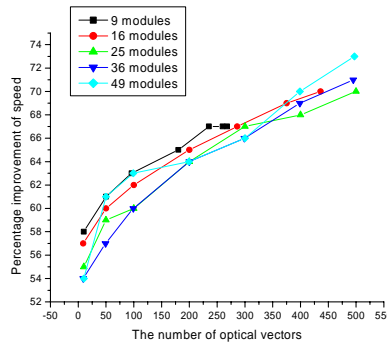
Figure 17. The graph for speed improvement versus optical directions with various numbers of modules

The results are very encouraging and show that more than 54% improvement in chip speed can be obtained through the use of optical interconnects.

Figure 18 shows the graph for the percentage saving of energy consumption versus the number of optical vectors with 9, 16, 25, 36 and 49 modules.
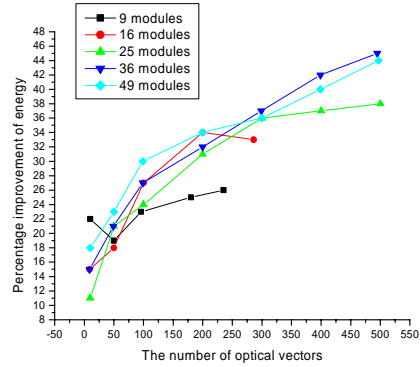
Figure 18. The graph for energy saving versus optical directions with various numbers of modules

In cases of 9 and 16 modules, the best results are with 235 and 200 optical interconnects respectively.

Table 4 shows results for optimization performed with 9, 16, 25, 36 and 49 modules against different number of optical directions supported by optical substrate. The table entries show the number of optimized optical vectors which must be less than the number of optical directions, the percentage saving in total energy consumption and the percentage improvement in overall SoC speed.

Table 4. The percentage improvement of energy consumption and speed with the different number of optical directions

Optical direction No. of module		10	50	100	200	300	400	500
9	Optical vector	10	50	96	180	235	260	268
	Energy (%)	22	19	23	25	26	20	15
	Speed (%)	58	61	63	65	67	67	67
16	Optical vector	9	50	100	200	286	375	436
	Energy (%)	15	18	27	34	33	31	26
	Speed (%)	57	60	62	65	67	69	70
25	Optical vector	9	49	100	199	300	396	489
	Energy (%)	11	21	24	31	36	37	38
	Speed (%)	55	59	60	64	67	68	70
36	Optical vector	9	49	99	200	299	399	495
	Energy (%)	15	21	27	32	37	42	45
	Speed (%)	54	57	60	64	66	69	71
49	Optical vector	10	50	99	199	300	399	497
	Energy (%)	18	23	30	34	36	40	44
	Speed (%)	54	61	63	64	66	70	73

3.1.4. Summary

In this research, a new approach to high performance SoC utilizing free-space optical interconnect was described. The results show that more than 55% improvement in overall SoC speed and more than 16% saving in total energy consumption are obtained on the average through the optimization process with the use of free-space optical interconnects. This translates to improve the overall SoC performance by a factor of more than 1.5.

3.2. BOSS (Board-level Optical clock Synthesis and Simulation tool)

Due to increasing levels of integration and sophistication in packaging technologies, the problem of routing electrical control and synchronization signals to the various subsystems of the package has assumed great significance. These control and synchronization signal networks, such as the clock distribution networks discussed in this paper, have to be designed very carefully in order to maximize the performance of the assembled electronic package while minimizing manufacturing costs. Specifically, for clock distribution, the skew of the clock signal from the source to the various destination points must be minimized very carefully in order to maximize the electrical performance of the package. In addition, overall power consumption must be minimized. These stringent design requirements necessitate the development of new CAD tools for emerging technologies such as optical interconnect.

In this research, we develop "BOSS" (Board-level Optical clock Synthesis and Simulator tool), a CAD tool that finds an optimal clock routing network and a best optical data input location for the network utilizing optical waveguide technology. Figure 19 shows the integration configuration of an optical clock routing on system-on-a-package (SOP) substrate.
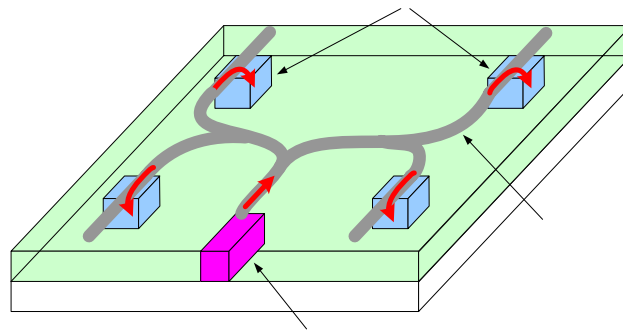
Figure 19. Integration configuration for high-speed optical clock distribution using embedded optoelectronics

The physical design of the optical clock distribution network is composed of three steps: partitioning, rough routing and calibration for clock skew. The three steps are described in detail in Section 3.2.2.1, 3.2.2.2 and 3.2.2.7.

3.2.1. Assumption

It is assumed that different combinations of L-shaped waveguides (90° bent L-shape) are used to construct the optimal optical routing network. This provides flexibility of design as opposed to the use of a rigid H-tree structure. The optical waveguide is assumed to be Transverse Electric (TE) field polarized with single mode operation. It is also assumed that there is an isolation layer between electrical and optical substrate to avoid signal-absorption. The final layout is a 1-to-2^x fanout structure where x>1. This means that the system is a single clock system and the number of detectors on board is 2^x where x>1.

From the latency point of view, optical interconnection has three types of latencies: transmitter latency, the time of flight and receiver latency. In this paper, the latencies in the optical transmitter and the optical receiver are not considered. However, it is reported that they are less than 100psec respectively in recent publication [30].

3.2.2. Optimization Algorithms

The optimization goals are as follows:

- *Given*: The locations of all the terminal points (detectors) to which the clock signal is to be routed optically.
- *Determine*: (a) The location of the clock signal transmitter on the printed wiring board and (b) the optimal layout of the optical waveguides from the transmitter to each of the detectors.
- *Such that (optimization criteria)*: (a) clock signal skew is minimized and (b) bending and propagation losses due to the optical waveguides are minimized.

The optimization algorithm consists of a layout partitioning, a waveguide routing and a local routing heuristic step. These are described next.

3.2.2.1. Layout Partitioning

The X-Y partition algorithm is used [26]. The board B is partitioned into two subregions, B_L and B_R with equal number of detectors. The subregions B_L and B_R are then partitioned in the orthogonal direction. Alternating x- and y-direction partitioning is recursively performed until there are two detectors in each subregion. The algorithm is illustrated in Figure 20.

Figure 20. X-Y partition algorithm
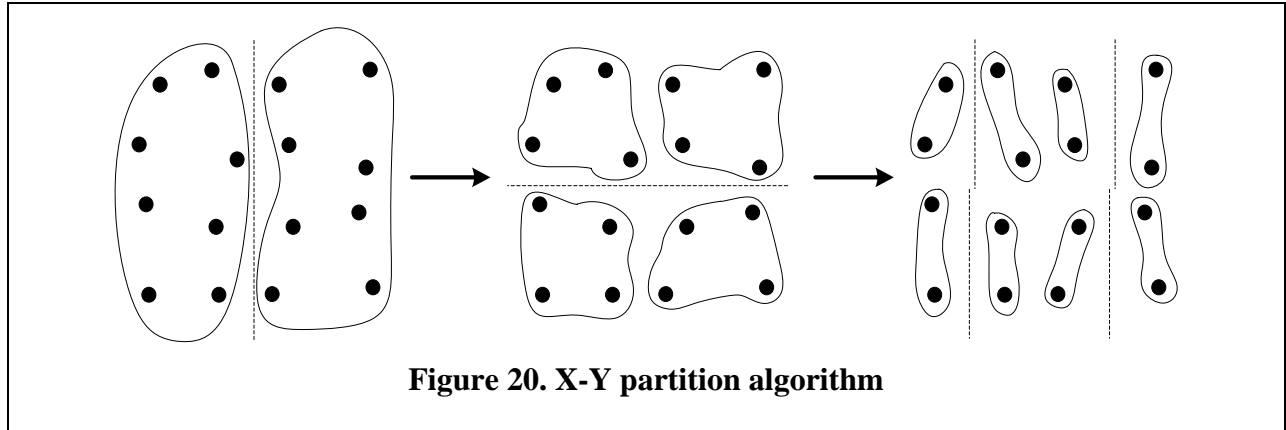
3.2.2.2. Waveguide Routing

For optical clock distribution, an algorithm which we call the Method of Optical Centroid Searching (MOCS) is used. The basic idea of the MOCS algorithm is to minimize the path length difference from the transmitter to any of the detectors by finding "optical centroid" based upon Manhattan Geometry. These optical centroids represent points in the layout grid that are equidistant from all other points in the same layout partition at each step of the recursive layout partitioning process. Hence, there are as many optical centroids as there are recursive calls in the layout partitioning algorithm. In order to feed all the detectors corresponding to a layout partition, the signal feeding the detectors is fanned out to the detectors or other optical centroids at the optical centroid corresponding to the partition. The MOCS algorithm is illustrated in Figure 21.

Figure 21. The method of optical centroid searching
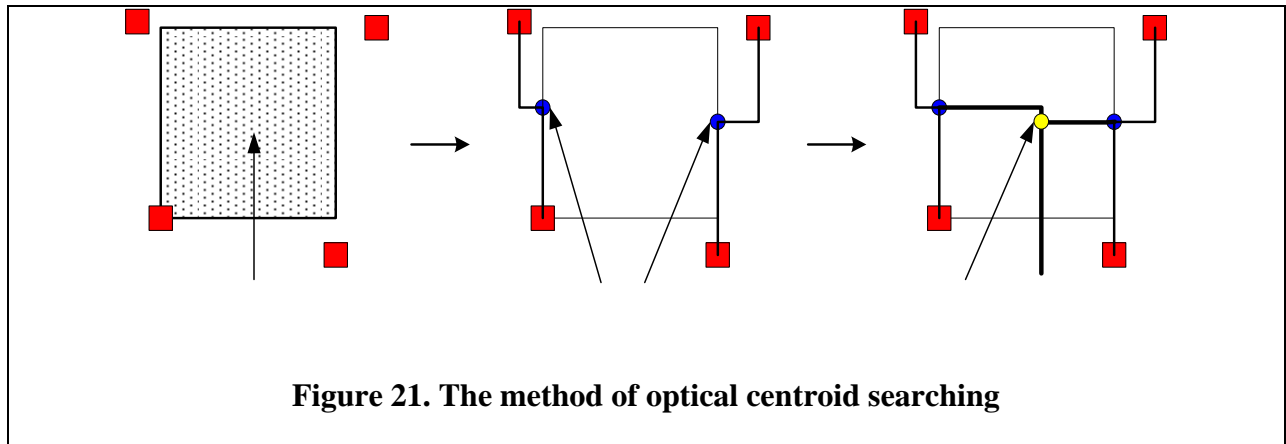
Let C be a set of 4 optical centroids. It is assumed that 4 detectors are initially set as the first optical centroids.

$$C(x) = \{c_x(i) \mid c(i) \text{ is centroid sorted in x-direction}\} \quad (5)$$

$$C(y) = \{c_y(i) \mid c_y(i) \text{ is centroid sorted in y-direction}\} \quad (6)$$

where $i = (1,2,3,4)$.

The next optical centroids of C are located in region R_C.

$$R_C = \{x, y \mid (c_x(2) \leq x \leq c_x(3)) \cap (c_y(2) \leq y \leq c_y(3))\} \quad (7)$$

Let C_L, C_R, C_T and C_B be initial optical centroids and C_M be the next optical centroid which is a yellow dot in
Figure 21. Let PL_L, PL_R, PL_T and PL_B be path lengths from the left, right, top and bottom optical centroid to the detectors on the left, right, top and bottom side.

The pseudo code for recursive MOCS is given in Figure 22. This MOCS are recursively introduced until there is only one optical centroid after searching.

```
Find_optical_centroid( )
1.   for (all the segments by X-Y partitioning ) {
2.       decide waveguide proceeding direction;
3.       if (waveguide proceeding direction is up or down) {
4.           abs_height = abs(CL(y) −CR(y));
5.           difference = abs(PLL–PLR);
6.           PL1 = PLL; PL2 = PLR; C1 = CL(y); C2 = CR(y);
7.       }
8.       else {
9.           abs_height = abs(CT(x)-CB(x));
10.          difference = abs(PLT–PLB);
11.          PL1 = PLT; PL2 = PLB; C1 = CT(x); C2 = CB(x);
12.      }
13.      if (PL1 > PL2) {
14.          if ((down and C1 < C2) or (up and C1 > C2)) {
15.              d1 = C1 − abs_height; d2 = C2 −difference;
16.          }
17.          else if ((down and C1 >= C2) or (up and C1 <= C2))  {
18.              d1 = C1; d2 = C2 −difference+ abs_height;
```

```
19.            }
20.         else if ((left and C_1 < C_2) or (right and C_1 > C_2)) {
21.              d_1 = C_1; d_2 = C_2 –difference– abs_height;
22.            }
23.         else {
24.              d_1 = C_1+ abs_height; d_2 = C_2 –difference;
25.            }
26.     else {
27.         if ((down and C_1 < C_2) or (up and C_1 > C_2)) {
28.              d_1 = C_1+difference– abs_height; d_2 = C_2;
29.            }
30.         else if ((down and C_1 >= C_2) or (up and C_1 <= C_2)) {
31.              d_1 = C_1+difference; d_2 = C_2+ abs_height;
32.            }
33.         else if ((left and C_1 < C_2) or (right and C_1 > C_2)) {
34.              d_1 = C_1+ abs_height; d_2 = C_2 –difference;
35.            }
36.         else {
37.              d_1 = C_1; d_2 = C_2– difference –abs_height;
38.            }
39.        }
40.     leng_diff = (d_2 – d_1)/2;
41.     if (waveguide proceeding direction is up or down) {
42.         C_M(x) = x1 + leng_diff;
43.         if (C_1 < C_2) C_M(y) = C_2;
44.         else C_M(y) = C_1;
45.        }
46.     else {
47.         C_M(y) = y1 + leng_diff;
48.         if (C_1 < C_2) C_M(x) = C_2;
49.         else C_M(x) = C_1;
50.        }
51.     Find_optical_centroid( );
52. }
53. Find the best location of an optical data input (Section 3.2.2.3);
```

**Figure 22. Pseudo code for MOCS algorithm**

For routing, any optical waveguide cannot cross any other optical waveguide or any detector to avoid inducing significant power loss caused by a discontinuity at the intersection.

3.2.2.3. Input Location

As mentioned earlier, the system designed in this paper is a single clock system. BOSS provides layouts of 1-to-2^x fanout (x>1). The optical data input location is determined at the end of routing through the MOCS (Method of Optical Centroid Searching) algorithm. The x coordinate is same as the last optical centroid and the y coordinate is the bottom of the board.

3.2.2.4. Bending Radius

Figure 23 shows a fundamental guided mode wavefront is traveling in an optical waveguide.

Figure 23. Bending loss derivation
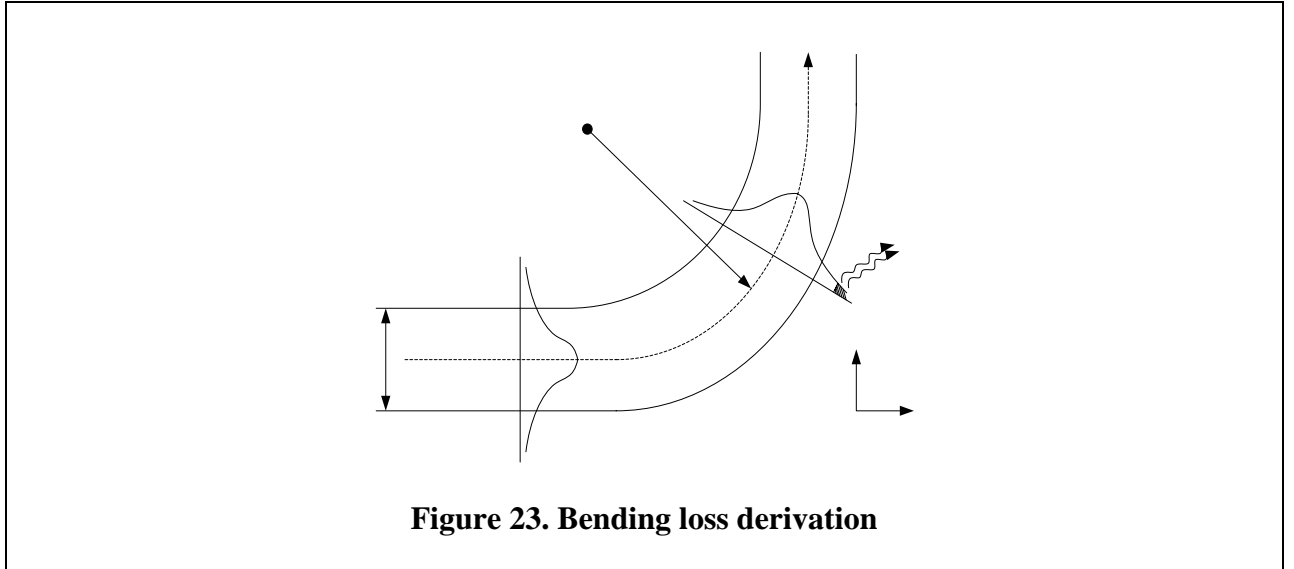
When the mode passes through the bent optical waveguide, tangential velocity of the mode in a cladding layer, $v_{tan}=R(d\theta/dt)$ will exceed the velocity of light. Thus, the portion of the evanescent field tail x_R cannot stay in phase and splits away from the guided mode and radiates into a cladding layer.

The rate of total power loss along z can be described by,

$$-\frac{dP_m(z)}{dz} = \alpha_m P_m(z) \qquad (8)$$

where α_m is the proportionality constant.

From Equation (8), the guided power for m^{th} mode can be written by,

$$P_m(z) = P_{0,m}e^{-2\alpha_m z} \qquad (9)$$

where $P_{0,m}$ is the incident power for m^{th} mode and $z=\pi R/2$.

The α_m can be easily derived by calculating radiating aperture [27].

$$\alpha_m = C_1 e^{-2C_2 R} \qquad (10)$$

where C_1 and C_2 are constants.

Therefore, Equation (9) is a function of bending radius of optical waveguide.

In order to minimize clock skew, BOSS finds the maximum bending radius with the assumptions that are made in Section 3.2.1. It means that path lengths are minimized and clock skews are also minimized with a given partitions and routing.

3.2.2.5. Loss Calculation

Two major loss terms in an index-guided optical interconnect are considered to evaluate layouts from BOSS simulation. The bending loss of optical waveguide is derived in the section 3.2.2.4. In order to specify to BOSS, the result of bending loss with specific parameters is curve-fitted with Boltzmann function. The parameters which are used in this paper are taken from a real fabrication condition [28]. They are 1μm Benzocyclobutene (BCB) as a core layer, SiO_2 as a cladding layer, 1μm waveguide thickness and a wavelength of 1.3μm. The analytical regression model for the bending loss of optical waveguide is shown in Equation (11).

$$BL = [1.0508/(1+e^{(radius-4\times10^{-5})/10^{-5}})] + 9.9\times10^{-4} \qquad (11)$$

Equation (11) tells that the result is saturated over 240μm bending radius of optical waveguide. It translates that the bending loss is negligible over 240μm bending radius. For the simulations, the minimum bending radius of optical waveguide is assumed to be 100μm.

The *propagation loss* caused by a scattering loss, material absorption and structural imperfection of optical waveguide can be estimated by using a fiber scanning method [28]. The measured propagation loss is 0.36dB/cm at a wavelength of 1.3μm.

In this paper, the *splitting loss* of optical waveguide is assumed to be negligible.

27

3.2.2.6. Delay Calculation

The effective refractive index of TE_0 mode in the dielectric waveguide is about 1.4927. c is the speed of light in free-space. n_{eff} is effective refractive index. v is the phase velocity of the guided mode in the material.

$$v = \frac{c}{n_{eff}} \approx 2 \times 10^8 \, (\text{m/s}) \qquad (12)$$

Thus, delay d is

$$d = \frac{x}{v} = \frac{x}{2 \times 10^8} (\text{sec}) \qquad (13)$$

where x = (a path length – the shortest path length).

However, the delay $d_{electrical}$ in electrical interconnection is

$$d_{electrical} = \frac{x}{c/5} = \frac{x}{0.6 \times 10^8} (\text{sec}) \qquad (14)$$

because the signal propagation speed for repeatered global electrical interconnections can be assumed to be approximately c/5 [29].

In order to minimize clock skew, the CAD algorithm finds the maximum bending radius with the assumptions that are made in Section 3.2.1. It means that path lengths are minimized and clock skews are also minimized with a given partitions and routing.

3.2.2.7. Local Routing Heuristic

For each optical centroid, the maximum bending radius is different. Examples of the local routing stage are shown in Figure 24.

Figure 24. Example layouts with different bending radii
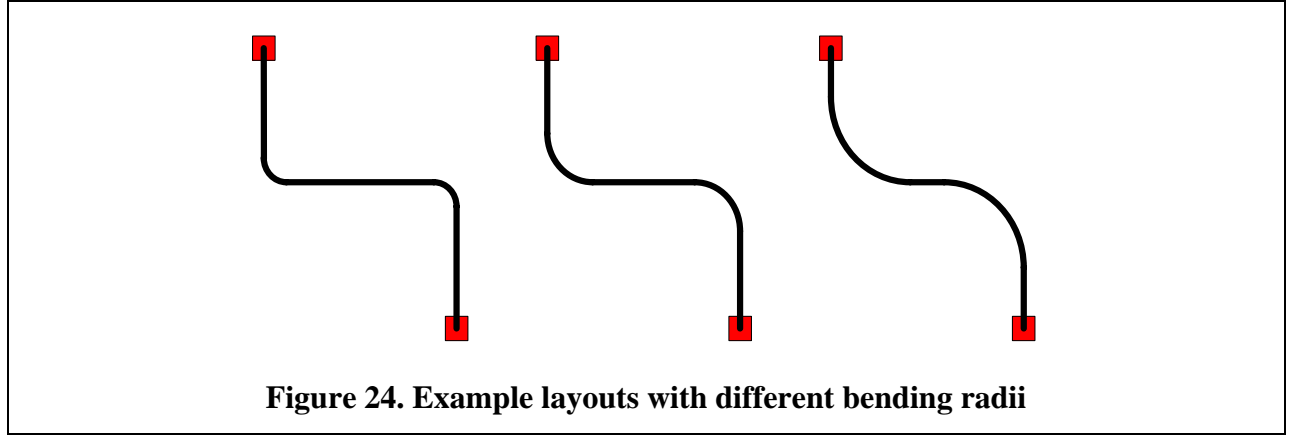
Different bending radius causes a length difference between optical data input and detector. This results in signal timing skew. Thereby, bending radii of all waveguides corresponding to the nth stage of recursion are all identical to avoid signal timing skew. The nth stage of recursion in Figure 22 corresponds to a local layout of the optical waveguides from a centroid (local centroid) to other centroids (sub-centroids) or a set of detectors. For routing from a local centroid to a sub-centroid, the ideal choice is to pick a waveguide layout with the largest bending radius. This minimizes bending losses. However, use of interconnect with different bending radius (see Figure 24) can cause timing skews between the various signal paths. Thus, all waveguides are routed using the smallest bending radius (of the largest for each interconnect) over all the interconnects from the local centroid to all the sub-centroids. This is called the local routing heuristic.

The pseudo code for local routing heuristic is as follows:

```
Local_routing_heuristic( )
1.  X-Y partitioning (Section 3.2.2.1);
2.  Find_optical_centroid( ) (Figure 21);
3.  for (each partition) {
4.      Find the optimal bending radius for the optical centroids at each partition;
5.      bending radius = the smallest bending radius among the optimal bending
        radii of each stage;
6.  }
7.  Calculate total loss (Section 3.2.2.5);
8.  Calculate delay (Section 3.2.2.6);
```

Figure 25. Pseudo code for local routing heuristic

3.2.3. Results and Analysis

3.2.3.1. Preliminary Result

The preliminary result for a 4-fanout structure is shown in Figure 26.
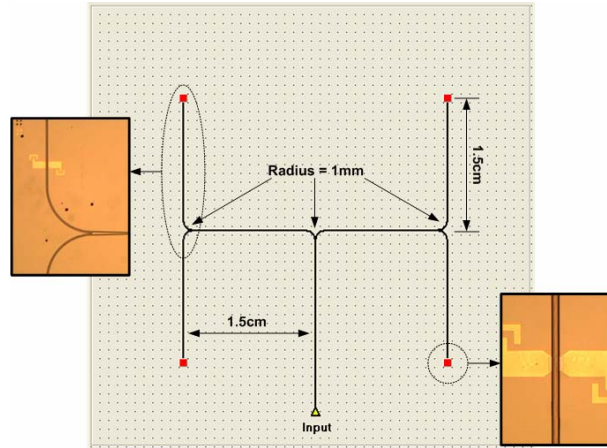
Figure 26. 1-to-4 H-tree structure layout with two enlarged microphotographs of fabrication

This design was designed using BOSS and fabricated. Two microphotographs corresponding to the fabricated Inverted-Metal Semiconductor Metal (I-MSM) photodetectors embedded in the BCB (Benzocyclobutene) polymer waveguide on the SiO$_2$/Si substrate are also shown in Figure

26. The dimension of the board is $5 \times 5 cm^2$. The bending radii of the optical waveguides are respectively 1 mm.

3.2.3.2. Symmetric Structure

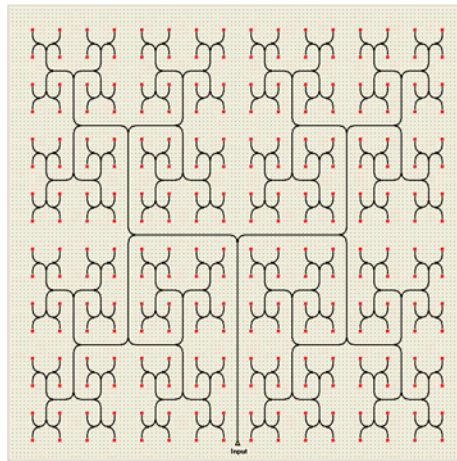An H-tree system with fanout of 256 has been designed. Figure 27 shows the unoptimized layout.

Figure 27. Symmetric clock routing of fanout 256 without optimization

The dimension of the board is $10 \times 10 cm^2$ and the bending radius is 1.5mm. The length between detectors is 6mm in the x- and y-directions.

The optimized layout of Figure 27 is shown in Figure 28 through the use of waveguides with different bending radii.
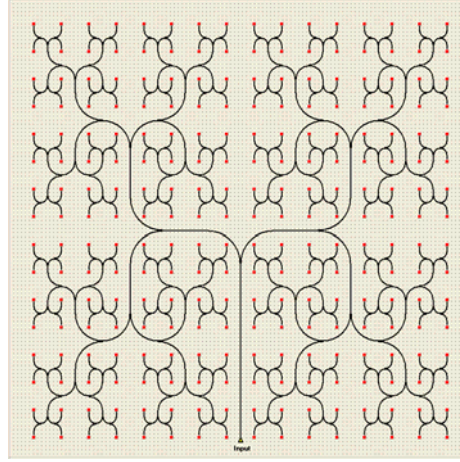
Figure 28. Symmetric clock routing of fanout 256 with optimization

This was carefully designed to avoid waveguide-crossing. The bending radii of each stage from a detector to an optical data input are 1.5, 1.5, 3, 3, 6, 6, 7 and 7mm. The total loss of the longest path from an optical data input to a detector due to changing bending radius is calculated and shown in Figure 29.
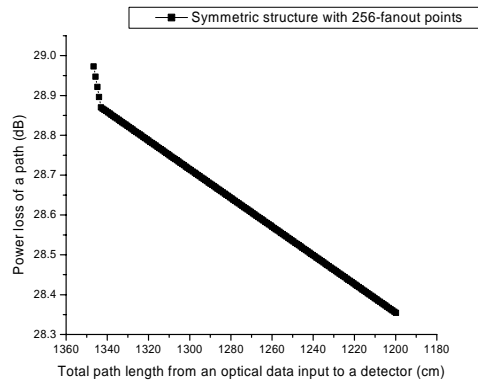
Figure 29. The reduction graph of total loss of the longest path from an optical data input to a detector

The total loss includes the bending loss of optical waveguide, the propagation loss and the splitting loss described in Section 3.2.2.5. The maximum power saving after optimization is about 15%.

3.2.3.3. Asymmetric Structure

With the new L-shaped optical waveguide, BOSS can design asymmetric structures while finding the best location of the optical data input.

Figure 30 shows an asymmetric clock routing of fanout 64 utilizing the proposed MOCS algorithm (see Section 3.2.2.2) with L-shape optical waveguide.
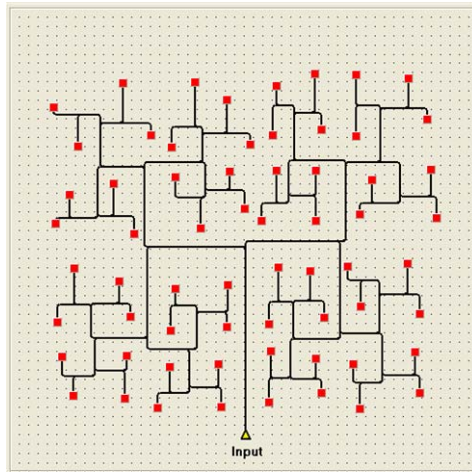
Figure 30. Asymmetric clock routing of fanout 64 without optimization

The dimension of the board is 5×5cm^2. Each bending radius is 200μm.

Through the use of different bending radii, the layout of Figure 30 is optimized and results in the layout of Figure 31.
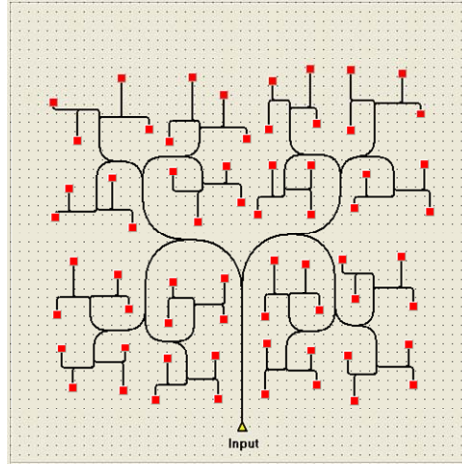
Figure 31. Asymmetric clock routing of fanout 64 with optimization

The bending radii of each stage from a detector to an optical data input are 0.2, 0.2, 1.5, 1.8, 4.2, and 5.0mm.

An asymmetric clock routing of fanout 256 is designed in Figure 32. The layout is very similar to the H-tree structure.

Figure 32. Asymmetric clock routing of fanout 256 without optimization

The dimension of the board is $10 \times 10 \text{cm}^2$. Each bending radius is 400μm.

Figure 33 is an optimized version of Figure 32 with different bending radii - note that no additional timing skew is introduced in Figure 33 as opposed to Figure 32.
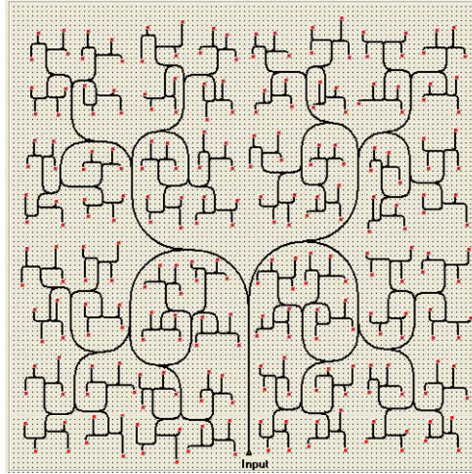
Figure 33. Asymmetric clock routing of fanout 256 with optimization

The bending radii of each stage from a detector to an optical data input are 0.4, 0.4, 1.5, 1.5, 4.8, 5.4, 10.8 and 11.6mm.

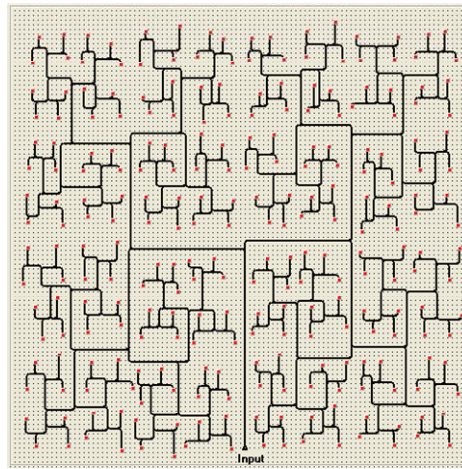Table 5 shows the total power loss along the longest path for each bending stage. As described earlier, the bending loss exceeded 240μm bending is negligible. That is the reason the results don't seem to be affected by the bending loss.

Table 5. Power loss along the longest path for each stage (dB)

Structure \ Stage		1	2	3	4	5	6	7	8
Symmetric	16	3.82	7.12	10.3	13.9	-	-	-	-
	64	3.84	7.12	10.3	13.4	16.5	20.1	-	-
	256	4.58	8.34	11.7	15.0	18.2	21.4	24.4	28.9
Asymmetric	64	3.99	7.90	11.2	14.3	17.4	21.0	-	-
	256	4.61	8.39	11.9	15.2	18.5	21.6	24.6	27.8

Table 6 shows minimum, maximum, average signal timing skew and the maximum time of flight along the longest path for different structures.

Table 6. Signal timing skew along the longest path

Structure / Skew		Minimum (psec)	Maximum (psec)	Average (psec)	Time of flight (psec)
Symmetric	16	0	0	0	163.91
	64	0	0	0	240.16
	256	0	0	0	599.89
Asymmetric	64	7.5	7.5	1.28	255.82
	256	23.9	26.1	3.48	614.38

The maximum signal timing skew is about 26.1psec when the time of flight is 614.38psec. This result implicates that signal timing skew in the simulation structures is negligible (< 4%). For the same structure with electrical interconnections based on Equation (14), the signal timing skew is about 87.43psec.

3.2.4. Summary

A new approach to optimized clock routing using optical waveguide is presented. The results are very encouraging and show that less than 26.1psec in signal timing skew is obtained for a signal flight time of 614.38psec. About 15% reduction in power consumption is also obtained over clock nets routed with existing (optical) methods.

4. Conclusion

We have presented two new approaches to design and optimization of optoelectronic systems using optical interconnections. The first approach is for data path routing on SoC utilizing free-space optical interconnect technology. The second approach is for clock routing between modules using optical waveguide interconnect. By taking into account various parameters, we have modeled optical interconnections. Using the models, data path routing and clock routing are

optimized by our new optimization algorithms. Experimental results show that our approaches can improve the overall performance of optoelectronic systems compared to conventional electrical systems in terms of system speed and energy consumption.

5. Published Papers

[1] **C. Seo** and **A. Chatterjee**, "*A CAD Tool for SoC Placement and Routing with Free-Space Optical Interconnect*," ICCD, pp. 24-29, September 2002.

[2] **C. Seo**, **A. Chatterjee** and T. J. Drabik, "*Wiring Optimization for Propagation Delay and Power Consumption of Multichip Modules with Free-Space Optical Interconnect*," ECTC, May 2003.

[3] J. Shin, **C. Seo**, A. Chellappa, M. Brooke, **A. Chatterjee** and N. M. Jokerst, "*Comparison of Electrical Interconnect and Optical Interconnect*," ECTC, May 2003.

[4] **C. Seo** and **A. Chatterjee**, "*Free-Space Optical Interconnect for High-Performance MCM Systems*", IWSOC, June 2003.

References

[1] "International technology roadmap for semiconductors 2002 update," Semiconductor Industry Association, 2002.

[2] D. A. Miller, "Rationale and challenges for optical interconnects to electronic chips," Proc. IEEE, vol. 88, no. 6, pp. 728-749, Jun. 2000.

[3] R. W. Keyes, "Power dissipation in information processing," Science, vol. 168, pp. 796-801, 1970.

[4] H. M. Gibbs, Optical Bistability: Controlling Light with Light. Orlando, FL: Academic, 1985.

[5] J. W. Goodman, F. J. Leonberger, S. Y. Kung, and R. A. Athale, "Optical interconnections for VLSI systems," Proc. IEEE, col. 72, no. 7, pp. 850-866, Jul. 1984.

[6] D. A. Miller, *et al*, "Bandedge electro-absorption in quantum well structures: The quantum confined stark effect," Phys. Rev. Letter, vol. 53, pp. 2173-2177, 1984.

[7] H. Soda, *et al*, "GaInAsP-InP surface emitting injection-lasers," Jpn. J. Appl. Phys., vol. 18, pp. 2329-2330, 1979.

[8] J. L. Jewell, *et al*, "Low-threshold electrically pumped vertical-cavity surface-emitting microlasers," Electron. Letter, vol. 25, pp. 1123-1124, 1989.

[9] T. J. Drabik, "Optoelectronic integrated systems based on free-space interconnects with an arbitrary degree of space-variance," Proc. IEEE, vol. 82, no. 11, pp. 1592-1622, Nov. 1994.

[10] G. I. Yayla, *et al*, "A Prototype 3D Optically Interconnected Neural Network," Proc. Of IEEE, vol. 82, no. 11, Nov. 1994.

[11] S. P. Levitan, *et al*, "Computer-Aided Design of Free-Space Opto-Electronic Systems," DAC, pp. 768-773, 1997.

[12] X. Zheng, *et al*, "High Speed Parallel Multi-chip Interconnection With Free Space Optics," International Conference on Parallel Interconnects, pp. 13-20, 1999.

[13] M. Forbes, J. Gourlay and M. Desmulliez, "Optically interconnected electronic chips: a tutorial and review of the technology," Electronics & Communication Engineering Journal, pp. 221-232, Oct. 2001.

[14] N. Savage, "Linking with Light," IEEE Spectrum, pp. 32-36, Aug. 2002.

[15] J. Wilson and J. F. B. Hawkes, Optoelectronics – An introduction, Prentice Hall, 1989.

[16] A short history of fiber optics. By Jeff Hecht, http://www.sff.net/people/Jeff.Hecht/history.html.

[17] B. D. Clymer and J. W. Goodman, "Timing uncertainty for receivers in optical clock distribution for VLSI," Opt. Eng., vol. 27, pp. 944-954, Nov. 1988.

[18] P. J. Delfyett, D. H. Hartman and S. Z. Ahmad, "Optical clock distribution using a mode-locked semiconductor laser-diode system," J. Lightwave Technology, vol. 9, pp. 1646-1649, Dec. 1991.

[19] J. H. Yeh, R. K. Kostuk and K. Y. Tu, "Board level H-tree optical clock distribution with substrate mode holograms," Jornal of Lightwave Technology, vol. 13, pp. 1566-1578, Jul. 1995.

[20] Y. Li, "Demonstration of fiber-based board-level optical clock distributions," International Conference on Massively Parallel Processing, pp. 224-228, 1998.

[21] B. Bihari, *et al*, "Optical clock distribution in super-computers using Polyimide-based waveguides," SPIE, vol. 3632, pp. 123-133, Jan. 1999.

[22] Travelling Salesman Problem Using Genetic Algorithms. http://www.lalena.com/ai/tsp/.

[23] N. A. Sherwani, Algorithms for VLSI physical design automation. Kluwer Academic Publishers, 1999.

[24] G. I. Yayla, P. J. Marchand, and S. C. Esener, "Speed and energy analysis of digital interconnections: comparison of on-chip, off-chip, and free-space technologies," Applied Optics, vol. 37, no. 2, pp.205-227, Jan. 1998.

[25] D. E. Goldberg, "Genetic algorithms in search, optimization, and machine learning," Addison-Wesley Publishing Company, 1989.

[26] M. A. B. Jackson, A. Srinivasan and E. S. Kuh, "Clock routing for high-performance ICs," DAC, pp. 573-579, Jun. 1990.

[27] D. L. Lee, Electromagnetic principles of integrated optics. New York Wiley, 1986.

[28] S. Y. Cho, S. W. Seo, M. A. Brooke and N. M. Jokerst, "Integrated Detectors for Embedded Optical Interconnections on Electrical Boards, Modules, and Integrated Circuits," IEEE Journal of Special Topics in Quantum Electronics, 2002.

[29] D. A. Miller, "Dense Optical Interconnections for Silicon Electronics" in Trends in Optics 1995, International Commission for Optics/ Academic Press, vol. 3, pp. 207-222, 1996.

[30] D. Agarwal, "Optical Interconnects to Silicon Chips using Short Pulses", Ph.D. Thesis, Stanford University, Sep. 2002.

[31] J. Cho, *et al*, "High performance MCM routing," IEEE DTC, pp. 27-37, Dec. 1993.

[32] H. B. Bakoglu, Circuit, Interconnects and Packaging for VLSI. Addison Wesley, 1990.

[33] M. Goets, "System on Chip Design Methodology Applied to System in Package Architecture," ECTC, pp.254-258, 2002.

[34] L. Benini and G. De Micheli, "Networks on chips: a new SOC paradigm," IEEE Computer, vol. 35, pp. 70-78, Jan. 2002.

[35] J. Becker, M. Glesner and T. Pionteck, **"**Adaptive systems-on-chip: architectures, technologies and applications," ICSD, pp. 2-7, 2001.

[36] Matsuzawa, "RF-SoC-expectations and required conditions," IEEE Tran. on Microwave Theory and Techniques, vol. 50, pp. 245-253, Jan. 2002.

[37] H. Lee, *et al*, "A New Formulation for SOC Floorplan Area Minimization Problem," DATE, 2002.

[38] J. Jahns, "Integrated free-space optical interconnects for chip-to-chip communications," Massively Parallel Processing, pp. 20-23, Jun. 1998.

[39] C. K. Cheng, *et al*, "Computer aided design and packaging optoelectronic systems with free space optical interconnects," Custom Integrated Circuits Conference, pp. 29.3.1-29.3.4, May 1993.

[40] J. A. Neff, "VCSEL-based smart pixels for free-space optical interconnection," LEOS, vol. 2, pp. 151-152, Nov. 1997.

[41] J. Davis, V. De and J. Meindl, "A Stochastic wire Length Distribution for Gigascale Integration(GSI)-part 1 : Derivation and Validation," Proc. IEEE Trans. On Electron Devices, vol. 45, no 3, pp. 580-589, Mar. 1998.

[42] M. R. Feldman, "Holographic optical interconnects for multichip modules," in Proc. SPIE, vol. 1390, pp.427-433, 1990.

[43] B. B. Bhattacharya, S. Das and S. C. Nandy, "High performance MCM routing: a new approach," VLSI Design, pp. 564-569, Jan. 1999.

[44] C. Sechen, "Chip-planning, placement, and global routing of macro/custom cell integrated circuits using simulated annealing," DAC, pp. 73-80, Jun. 1988.

[45] V. Schnecke and O. Vornberger, "Genetic design of VLSI-layouts," GALESIA, pp. 430-435, Sep. 1995.

[46] N. G. Bourbakis and M. Mortazavi, "An efficient building block layout methodology for compact placement," VLSI, pp. 118-123, Mar. 1995.

[47] C. S. Baldwin, *et al*, "High performance package designs for a 1 GHz microprocessor," IEEE Trans. on Advanced Packaging, vol. 24, pp. 470-476, Nov. 2001.

[48] J. Lienig, M. N. S. Swamy and K. Thulasiraman, "Routing algorithms for multi-chip modules," DAC, pp. 286-291, Sep. 1992.

[49] K. Bois, *et al*, "Optimizing the package design with electrical modeling and simulation," ECTC, pp. 111-117, 2001.

[50] C. L. Valenzuela and P. Y. Wang, "VLSI Placement and Area Optimization Using a Genetic Algorithm to Breed Normalized Postfix Expressions," IEEE Trans. on Evolutionary Computation, vol. 6, no. 4, pp. 390-401, Aug. 2002.

[51] J. Cong, A. B. Kahng and G. Robins, "Matching-Based Methods for High-Performance Clock Routing," IEEE TCAD, vol. 12, no. 8, pp. 1157-1169, Aug. 1993.

[52] S. L. Sam, A. Chandrakasan and D. Boning, "Variation issues in on-chip optical clock distribution," IEEE International Workshop on Statistical Methodology, pp. 64-67, 2001.

[53] W. H. Ryu, *et al*, "Over GHz low-power RF clock distribution for a multiprocessor digital system," ECTC2001, pp. 133-140, 2001.

[54] R. T. Chen, *et al*, "Fully embedded board-level guided-wave optoelectronic interconnects," Proceedings of the IEEE, vol. 88, pp. 780-793, Jun. 2000.

[55] A. V. Mule, *et al*, "An optical clock distribution network for gigascale integration," Interconnect Technology Conference 2000, pp 6, 2000.

[56] K. J. Ebeling, "VCSELs: prospects and challenges for optical interconnects," LEOS2000, vol. 1, pp. 7-8, 2000.

[57] S. Tanp, et al, "1-GHz clock signal distribution for multi-processor super computers," International Conference on Massively Parallel Processing Using Optical Interconnections, pp. 286-191, 1996.

[58] H. Zarschizky, *et al*, "Optical Clock Distribution With A Compact Free Space Interconnect System," LEOS1992, pp. 590-591, 1992.

[59] C. Sebillotte and T. Lemoine, "Computer generated holograms directly etched in glass and their use as boards interconnects means," Holographic Systems, Components and Applications, pp. 52-56, 1991.

[60] D. Prongue and H. P. Herzig, "Design and fabrication of HOE for clock distribution in integrated circuits," Holographic Systems, Components and Applications, pp. 204-208, 1989.

[61] A. Naeemi, P. Zarkesh-Ha, C. S. Patel, and J. D. Meindl, "Performance improvement using on-board wires for on-chip interconnects," EPEP2000. pp 325-328, Oct. 2000.

[62] N. A. Kurd, J. S. Barkatullah, R. O. Dizon, T. D. Fletcher, and P. D. Madland, "A multi-GHz clocking scheme for Pentium 4 microprocessor," IEEE J. Solid State Circuits, vol. 36, pp. 1647-1653, Nov. 2001.

[63] R. K. Krishnamurthy, K. Soumyanath, and S-L. Lu, "High-performance interconnect design for system-on-chip," Proc. IEEE International ASIC/SOC Conference, pp. 424, Sept. 1999.

[64] S. K. Tewksbury and L. A. Hornak, "Optical clock distribution in electronic systems," J. VLSI Signal Processing, vol. 16, pp. 225-246, June-July 1997.

[65] S. J. Walker and J. Jahns, "Optical clock distribution using integrated free-space optics," Opt. Communications, vol. 90, pp. 359-371, June 1992.

[66] K. M. Carrig, *et al*, "A clock methodology for high-performance microprocessors," J. VLSI Signal Process., vol. 16, pp. 217-224, Jun. 1997.

[67] R. R. Tummala, Fundamentals of Microsystems Packaging. McGraw-Hill, 2001.